International Journal of Fluid Machinery and Systems
Vol. 4, No. 4, October-December 2011

DOI: http://dx.doi.org/10.5293/IJFMS.2011.4.4.387
ISSN (Online): 1882-9554

Original Paper

Radial Thrust of Single-Blade Centrifugal Pump

Yasuyuki Nishi[1], Junichiro Fukutomi[2] and Ryota Fujiwara[3]

[1]Department of Mechanical Engineering, Ibaraki University
4-12-1 Nakanarusawa-cho, Hitachi-shi, Ibaraki, 316-8511, Japan
[2]Institute of Technology and Science, The University of Tokushima
2-1 Minamijosanjima-cho, Tokushima-shi, Tokushima, 770-8506, Japan
[3]Graduate School of Advanced Technology and Science, The University of Tokushima
2-1 Minamijosanjima-cho, Tokushima-shi, Tokushima, 770-8506, Japan

Abstract

Single-blade centrifugal pumps are widely used as sewage pumps. However, the impeller of a single-blade pump is subjected to strong radial thrust during pump operation because of the geometrical axial asymmetry of the impeller. Therefore, to improve pump reliability, it is necessary to quantitatively understand radial thrust and elucidate the behavior and mechanism of thrust generating. This study investigates the radial thrust acting up on a single-blade centrifugal impeller by conducting experiments and CFD analysis. The results show that the fluctuating component of radial thrust increases as the flow rate deviates from the design flow rate to low or high value. Radial thrust was modeled by a combination of three components, inertia, momentum, and pressure by applying an unsteady conservation of momentum to the impeller. The sum of these components agrees with the radial thrust calculated by integrating the pressure and the shearing stress on the impeller surface. The behavior of each component was shown, and the effects of each component on radial thrust were clarified. The pressure component has the greatest effect on the time-averaged value and the fluctuating component of radial thrust. The time-averaged value of the inertia component is nearly 0, irrespective of the change in the flow rate. However, its fluctuating component has a magnitude nearly comparable with the pressure component at a low flow rate and slightly decreased with the increase in flow rate.

Keywords: Turbomachinery, Centrifugal Pump, Sewage pump, Single-Blade, Radial Thrust, CFD

1. Introduction

Given that a sewage pump is used for the transportation of liquids containing solids and fibrous foreign bodies, a high performance in passing foreign bodies is required. A single-blade centrifugal pump can form a large passed particle size (the minimum particle size for the flow channel in a pump); thus, it is commonly used as a sewage pump. However, a large radial thrust is imparted to the impeller of a single-blade centrifugal pump during operation [1,2]. This radial thrust causes vibrations of the pump shaft, reducing the service life of bearings and shaft seal devices. Therefore, it is extremely important to understand this radial thrust quantitatively and to clarify its behavior and the mechanism of generation in order to improve pump reliability.

With respect to centrifugal pumps, many studies have investigated time-averaged radial thrust resulting from the asymmetry of the volute casing [3-5] as well fluctuating radial thrust [6]. It has been reported that a fluid dynamics imbalance occurs in multi-blade centrifugal impellers as a result of geometrical manufacturing errors [7]. However, with a single-blade centrifugal pump, the impeller itself is inherently geometrically asymmetric. Furthermore, installing a volute casing without axial symmetry around an impeller makes the pressure distribution around the impeller even more uneven and causes significant radial thrust. In the case of radial thrust on single-blade centrifugal pumps, studies have been conducted to understand the effects of the number of blades [1,8], the effects of blade angle distributions [9], and the effects of casings [1,9]. Moreover, pressure distributions on the blade surfaces have been measured to investigate the mechanism of the occurrence of fluctuating radial thrust [2]. However, details of the behavior and mechanism of generation of radial thrust in a single-blade centrifugal pump are yet to be elucidated.

This study aims at elucidating the behavior and mechanism of generation of radial thrust in a single-blade centrifugal pump by means of experiments and CFD analysis. Therefore, the behavior of radial thrust in the single-blade centrifugal impeller constructed on the basis of the design method proposed in a previous report [10] was investigated. The law of conservation of unsteady momentum was applied to the impeller, and the components of the radial thrust acting on the impeller were modeled. As a result, the effects of these components on radial thrust were clarified.

Received October 12 2011; revised November 2 2011; accepted for publication December 8 2011: Review conducted by Prof. Yulin Wu. (Paper number O11021C)
Corresponding author: Yasuyuki Nishi, Professor, y-nishi@mx.ibaraki.ac.jp

2. Experimental Apparatus and Method

Figure 1 shows a schematic diagram of the test impeller, and its associated technical data is given in Table 1. The test impeller is a single-blade centrifugal impeller with a passed particle size constructed using a design method proposed in a previous report [10].

Figure 2 shows a schematic diagram of the experimental apparatus. The flow rate Q was adjusted by a gate valve on the discharge side, and was measured using an electromagnetic flow meter. The total head H was determined by measuring the static pressure using small-strain-gage-type pressure transducers attached to the static pressure holes before and after the pump. The shaft power L was determined by separately measuring the rotational speed n with an electromagnetic pickup, and the driving torque T with a torsion-bar-type torque detector. The experiment was conducted at a rotational speed of n = 1740 min^{-1}.

In the coordinate system shown in Fig. 3, the directions parallel and perpendicular to the volute casing were defined as the X- and Y-axes, respectively. With the impeller phase angle θ_0 taken anticlockwise from the X-axis, the position at which the blade outlet end passes the X-axis (the position shown in Fig. 3) was defined as $\theta_0 = 0°$.

Eight points for measuring pressure fluctuations were located at a distance of 10 mm outward from the impeller outlet, as shown in Fig. 3, at intervals of 45°, starting at θ = 22.5°, in the anticlockwise direction with θ = 0° set on the X-axis. When the blade outlet end was at $\theta_0 = 0°$, a trigger signal was generated and the measurement of pressure fluctuation was synchronized with the rotation of the impeller.

The X-Y load cell shown in Fig. 4 was included in the bearing perimeter, and the measurement of radial thrust was synchronized with the rotation of the impeller. A strain gauge was mounted on the X-Y load cell in the four-active-gauge method. The dynamic calibration method [11] was adopted for calibration. To calibrate the relation between the output voltage and force, a known centrifugal force was applied in air on the calibration disk with a mass equal to the impeller mass minus the buoyancy acting on the impeller. The test impeller and the calibration disk were in dynamic balance. The influence of heat on the bearing section was nullified by using a measuring method in which the pump was stopped for a short time of about 15 second under thermally stable conditions to adjust the zero point and was immediately brought back to operation under the same conditions [12].

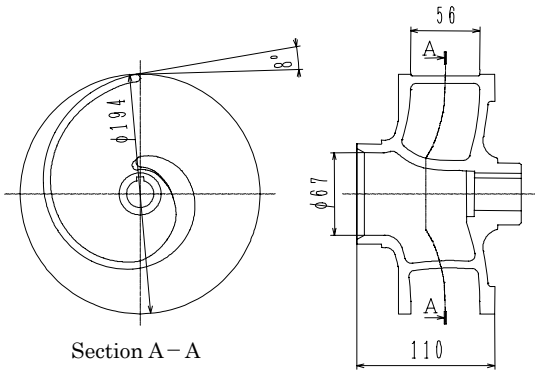

Fig. 1 Test impeller

Table 1 Specification of the impeller

Impeller suction diameter D_0	67 mm
Impeller inner diameter D_1	58 mm
Impeller outer diameter D_2	194 mm
Impeller inlet width b_1	56 mm
Impeller outlet width b_2	56 mm
Impeller inlet angle β_{1b}	13 °
Impeller outlet angle β_{2b}	8 °

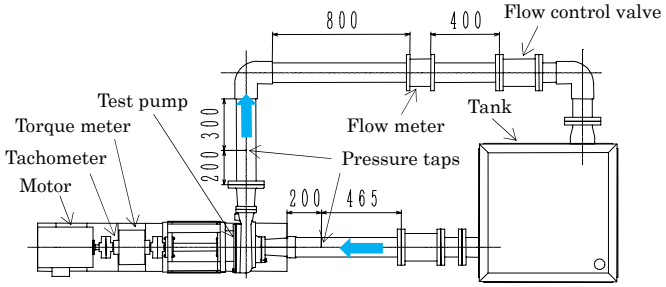

Fig. 2 Experimental apparatus

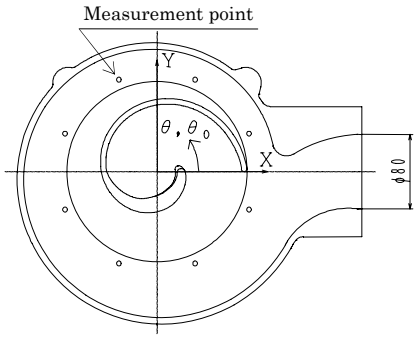

Fig. 3 Measurement points

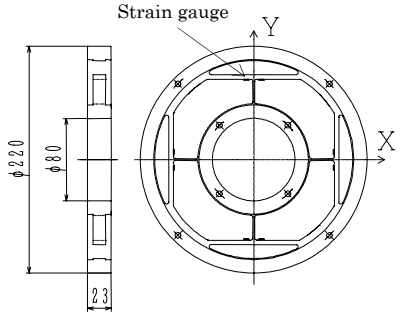

Fig. 4 X-Y Load cell

3. Method and Conditions of Analysis

FLUENT 6.3, general-purpose analysis code, was used in this study. Three-dimensional unsteady flow analysis was conducted in consideration of the mutual interference of the impeller and the volute casing [13]. In this analysis, the standard wall function was used to handle regions near wall surfaces, and the standard k–ε model was adopted as the turbulent flow model.

The computational domain consists of a suction pipe, an impeller, a volute casing, and a discharge pipe, with the total number of elements reaching about 900,000, as shown in Fig. 5. In this study, the gaps between the impeller and the volute casing were not modeled.

The inlet and outlet of the computational domain were the suction pipe inlet and the discharge pipe outlet, respectively. As boundary conditions, the mass flow rate was given to the inlet boundary, and a gauge pressure of 0 Pa was given to the outlet boundary. The same angular velocity as in the experimental conditions was given to the fluid domain of the impeller in a rotational coordinate system. The impeller surface and the rear and front shroud walls were defined in a relative coordinate system; the suction pipe, the volute casing, and the discharge pipe were defined on a fixed wall in an absolute coordinate system. To bond the outlet of the suction pipe to the suction inlet of the impeller and the outlet of the impeller to the inlet of the volute casing, the sliding mesh method [14] was used.

4. Experimental and Analytical Results and Discussion

4.1 Performance Characteristics

Figure 6 compares the performance curves of the test pump obtained experimentally and analytically. Figure 6 also shows the design points for the impeller, the theoretical head H_{th} for a finite number of blades, and the volute characteristic equation [15]. In this case, H_{th} was determined by means of a method that used the shaft power [16]. There is good agreement between the experimental and analytical values of the head coefficient ψ. The head curve does not have a positively sloped instability characteristic. The experimental pump efficiency η is 62%. However, the best efficiency point is located near $\varphi = 0.030$; this value of φ is greater than the design flow rate value of 0.019. This is because of poor matching between the impeller and the volute casing, as is clear from the fact that the intersection of H_{th} and volute characteristic equation is at a flow rate greater than the design flow rate. It seems that the error of the efficiency of the experimental value and the analytical value is also large in the best efficiency point flow rate under this influence.

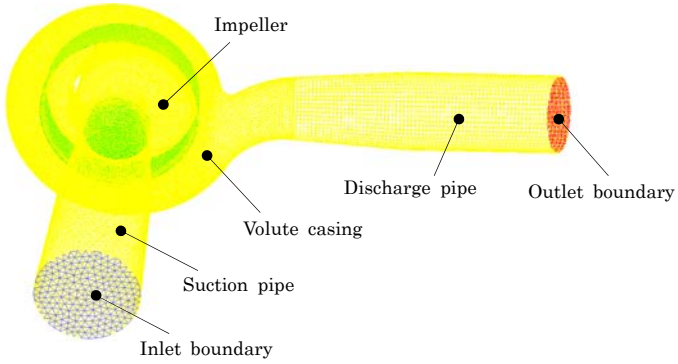

Fig. 5 Computational domain and grids

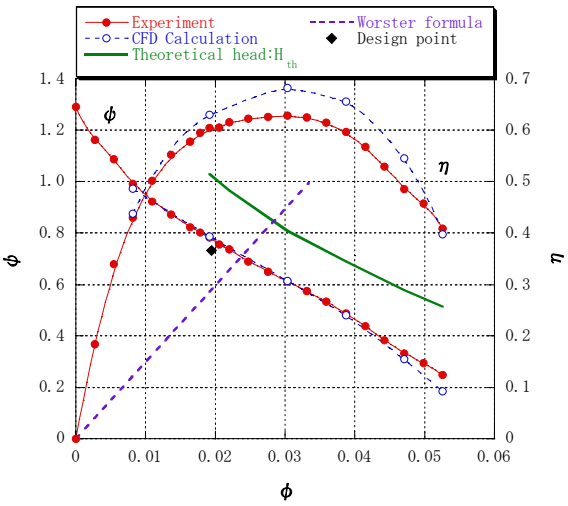

Fig. 6 Performance curves

4.2 Comparison of Radial Thrust

Radial thrust can be expressed as a vector sum of the averaged component (time-averaged value) based on the volute casing and the fluctuating component based on the impeller itself [1,2,11]. This study defines the vector difference between the radial thrust F and its averaged component F_{av} as the fluctuating component ΔF, which is discussed below.

Figures 7(a) and 7(b) compare the Lissajous figures for the experimental radial thrust F obtained through the X-Y load cell and analytical F obtained through the CFD analysis, at the design flow rate $\varphi = 0.019$ and the best efficiency point flow rate $\varphi = 0.030$, respectively. The analytical radial thrust was obtained using the following equation.

$$F_i = \int_A P(i \cdot n) dA + \int_A \mu \frac{dw}{dn} \cdot i dA \tag{1}$$

Here, F_i denotes the fluid force on A in i-direction, i denotes the unit vector in i-direction, n denotes the unit vector perpendicular to A, and μ denotes the viscosity [Pa·s]. As the gaps between the impeller and the volute casing are not modeled, the outer shroud surfaces are not included in A. That is, the area of the impeller A consists of is the blade pressure surfaces, the blade suction surfaces, and the inner shroud surfaces. In Figs. 7(a) and 7(b), the values of radial thrust at $\theta_0 = 0°$, 90°, 180°, and 270° are

denoted by ●, ▲, ■, and ◆, respectively, and the time-averaged values for radial thrust are denoted using the same notation system. These notational conventions are adopted in the illustrations below.

Figures 7(a) and 7(b), respectively, show that for $\varphi = 0.019$ and $\varphi = 0.030$, each radial thrust rotates anticlockwise around the time-averaged value as the impeller rotates, with a closed curve delineated during a rotation of the impeller. A comparison between the experimental and analytical values, shown in Fig. 7(a) for $\varphi = 0.019$, reveals that the Lissajous figure for the analytical values exhibits a shape close to a perfect circle, while that for the experimental values exhibits a slightly flatter shape. The experimental and analytical time-averaged values approximately agree, and show a relatively good agreement, although values of the fluctuating component ΔF show a slight difference in both the magnitude and direction. On the other hand, for the best efficiency point flow rate $\varphi = 0.030$, the experimental and analytical ΔF values show a slight difference, which leads to a slight difference in the time-averaged values. The difference in the radial thrust between the experimental and analytical values is caused by a remarkable difference at $0° < \theta_0 < 90°$. This difference is considered to be the influence of the interference between the volute tongue region and the impeller. Furthermore, because the gaps between the impeller and the volute casing and the whirling motion of the impeller are not modeled in the CFD analysis, the force acting on the rear and front shrouds and the rotordynamic force are not taken into consideration. For these reasons, the experimental value of radial thrust is larger than the analytical values and exhibits a flatter shape.

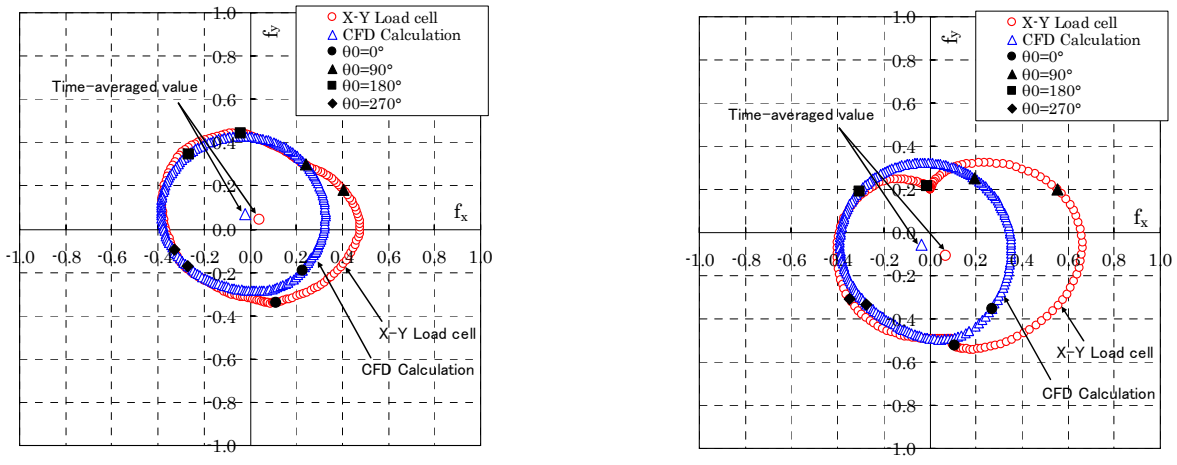

(a) φ = 0.019 (b) φ = 0.030

Fig. 7 Lissajous figures of radial thrust

4.3 Behavior of Radial Thrust as a Result of Change in Flow Rate

Figures 8(a) and 8(b) respectively show the Lissajous figures for the experimental and analytical values of radial thrust F accompanying the change in flow rate. An observation of the change in the time-averaged values of radial thrust accompanying the change in flow rate shown in Figs. 8(a) and 8(b) clearly shows that the experimental and analytical values exhibit the same trends and agree qualitatively. As seen from the time-averaged pressure distribution around the impeller shown in Fig. 9, this is because at a flow rate lower than the design flow rate the pressure becomes low in the volute tongue region and high in the volute outlet region. As a result, force is exerted in the +Y direction. At flow rate larger than the design flow rate, the pressure becomes low in the volute outlet region and high in the volute tongue region. As a result, force is exerted in the -Y direction. As known from previous studies [1,2,11], it is confirmed that the time-averaged value of radial thrust is affected greatly by the time-averaged pressure, i.e., the volute casing. Moreover, it is shown that the time-averaged experimental and analytical values in Fig. 9 agree satisfactorily at all flow rates.

Figure 8(a) reveals that the experimental ΔF becomes minimum at the design flow rate $\varphi = 0.019$. The ΔF increases as the flow rate deviates from the design flow rate and at a flow rate larger than the design flow rate, the Lissajous figure adopts an uneven form. As Fig. 8(b) shows, the analytical ΔF increases as the flow rate deviates from $\varphi = 0.019$. As shown above, the experimental and analytical radial thrust values agree qualitatively. However, at a flow rate larger than the design flow rate, the Lissajous figure for the analytical value does not take as uneven shape as that for the experimental values. Moreover, the analytical ΔF is slightly smaller.

4.4 Modeling of Radial Thrust Components

The results shown thus far revealed that the radial thrust of a pump changes its behavior considerably as the flow rate changes. With this in mind, we attempt to model the components of radial thrust and try to understand them quantitatively.

On the basis of the law of conservation of unsteady momentum, the radial thrust F that acts on the blade pressure surfaces, the blade suction surfaces, and the inner shroud surfaces is modeled by the following equation.

$$F = F_I + F_M + F_P \tag{2}$$

Here, F_I denotes the inertia component [N], F_M denotes the momentum component [N], and F_P denotes the pressure component [N]. Radial thrust by shearing stress is ignored.

The x and y components of the inertia component F_I, which is a force generated by the change of momentum of the impeller per unit time, are given by the following equations.

$$F_{Ix} = -\rho \int_V \frac{dv_x}{dt} dV \tag{3}$$

$$F_{Iy} = -\rho \int_V \frac{dv_y}{dt} dV \tag{4}$$

Here, V denotes the inspection volume, i.e., the volume of the flow channel in the impeller [m^3].

The x and y components of the momentum component F_M, which is a force generated by the difference between the momentum flowing out of the impeller outlet per unit time, and the momentum flowing in from the impeller suction inlet per unit time, are given by the following equations.

$$F_{Mx} = -\rho \left(\int_{A_2} v_{x2} v_{r2} dA - \int_{A_0} v_{x0} v_{a0} dA \right) \tag{5}$$

$$F_{My} = -\rho \left(\int_{A_2} v_{y2} v_{r2} dA - \int_{A_0} v_{y0} v_{a0} dA \right) \tag{6}$$

The x and y components of the pressure component F_P, which is a force resulting from the pressure acting on the fluid on the inspection surface, are given by the following equations.

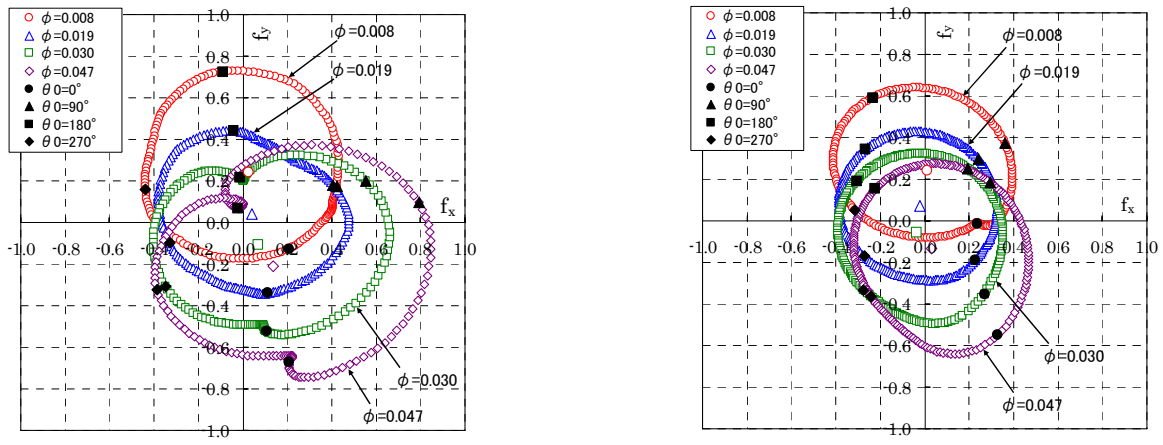

(a) Experiment (b) CFD Calculation

Fig. 8 Changes of radial thrust

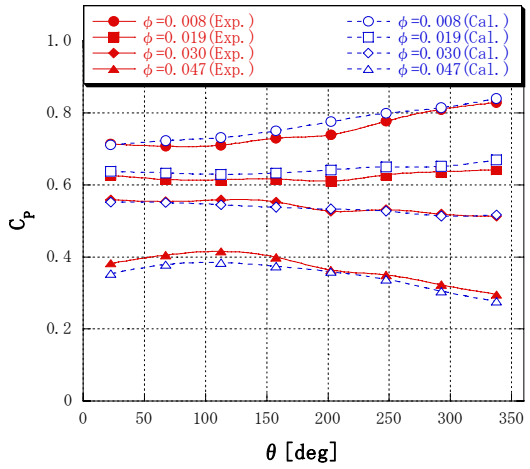

Fig. 9 Time-averaged pressure distributions around the impeller

$$F_{Px} = -\int_{A_2} P_2 \cos\theta dA \tag{7}$$

$$F_{Py} = -\int_{A_2} P_2 \sin\theta dA \tag{8}$$

By using the above equations, the x and y components of the radial thrust acting on the impeller are given by the following equations.

$$F_x = -\rho\int_V \frac{dv_x}{dt}dV - \rho(\int_{A_2} v_{x2}v_{r2}dA - \int_{A_0} v_{x0}v_{a0}dA) - \int_{A_2} P_2 \cos\theta dA \tag{9}$$

$$F_y = -\rho\int_V \frac{dv_y}{dt}dV - \rho(\int_{A_2} v_{y2}v_{r2}dA - \int_{A_0} v_{y0}v_{a0}dA) - \int_{A_2} P_2 \sin\theta dA \tag{10}$$

4.5 Result of Analysis of Radial Thrust Components

Figures 10(a) and 10(b) compare the Lissajous figures for F obtained by component analysis and direct integration, at the design flow rate $\varphi = 0.019$ and at the best efficiency point flow rate $\varphi = 0.030$, respectively. However, in calculating the pressure component F_P of the component analysis value, the static pressure of the wall surface on the shroud side was used as the static pressure at the impeller outlet, with the static pressure assumed to be constant in the direction of width. At both flow rates, the component analysis value is slightly larger than the direct integration value (CFD Calculation). However, both agree well in terms of the time-averaged values and the magnitude and direction of the fluctuating components. The reason for the component analysis value being slightly larger is thought to be the absence of the effect of shearing stress and the effect of the width-direction distribution of the static pressure at the impeller outlet. As the component analysis value agrees well with the direct integration value, the modeling of the radial thrust components is thought to be appropriate. In the following, therefore, the different components are examined in detail.

Figures 11(a) to 11(c) show the change in each component accompanying the change in flow rate, as determined from the CFD analysis. In Fig. 11(a), the Lissajous figures for the inertia components are about the same shape at each flow rate. It is clear from the figure that the time-averaged value of the inertia component is located nearly at the origin despite changes in the flow rate and that its fluctuating component ΔF_I rotates in the rotational direction of the impeller as the impeller rotates. The direction of ΔF_I at $\theta_0 = 0°$ is about the same for each flow rate, showing that the direction of ΔF_I changes only slightly with change in flow rate. The magnitude of ΔF_I slightly decreases with an increase in the flow rate. However, it is clear from the figure that the magnitude of ΔF_I is such that it cannot be neglected in radial thrust.

In Figure 11(b), although a different trend is shown at $\theta_0 = 0°$ at a flow rate $\varphi = 0.047$, which is larger than the design flow rate, the momentum component rotates around its time-averaged value in the direction of the rotation of the impeller at other flow rates. The change in the time-averaged values of the momentum component is different from the change in the time-averaged values of the radial thrust as shown in Fig. 8. In addition, the magnitude of the fluctuating component ΔF_M of the momentum component is considerably smaller than the magnitude of the fluctuating components of other components, and it further decreases as the flow rate increases.

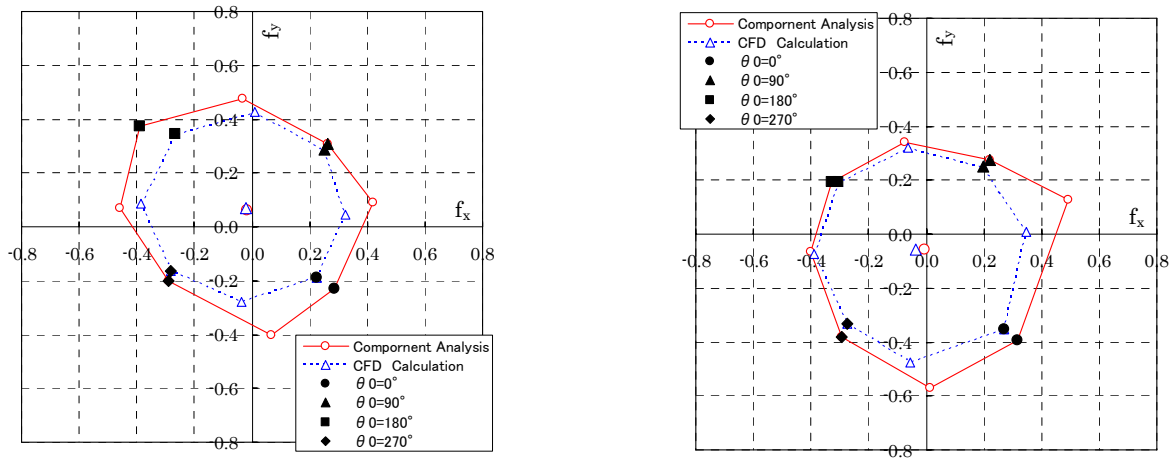

(a) φ = 0.019 (b) φ = 0.030

Fig. 10 Lissajous figures of radial thrust

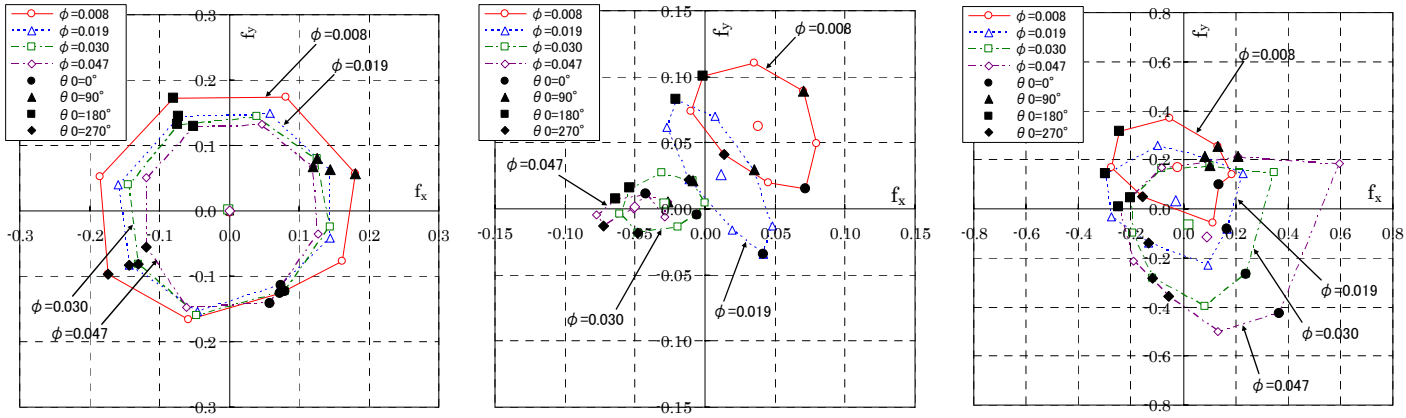

(a) Inertia component (b) Momentum component (c) Pressure component

Fig. 11 Changes of each component (CFD)

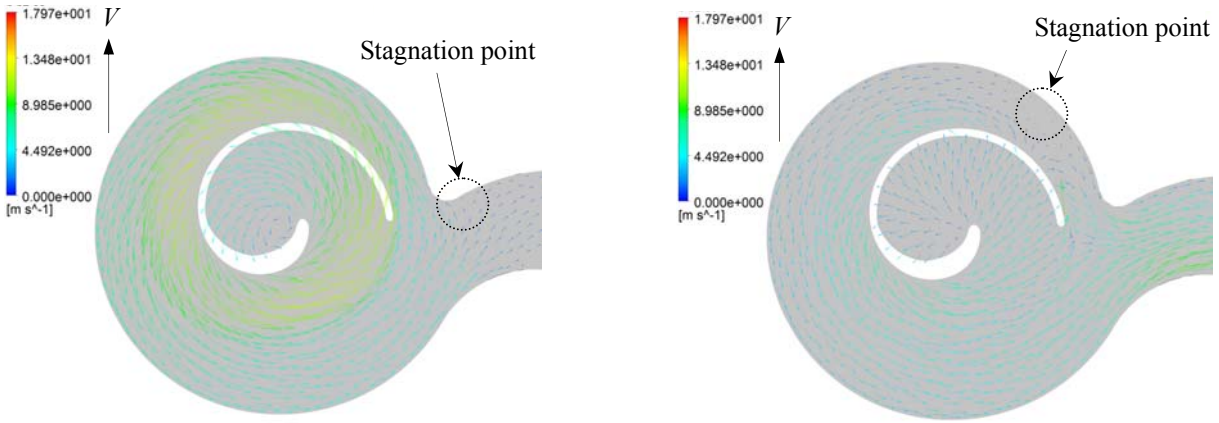

(a) φ = 0.008 (b) φ = 0.047

Fig. 12 Absolute velocity vectors ($\theta_0 = 0^\circ$)

Figures 12(a) and 12(b) show the results of the CFD analysis on the absolute velocity vectors at the cross section at the width center b/b_2 of the impeller outlet at different flow rates at $\theta_0 = 0^\circ$. At a low flow rate $\varphi = 0.008$, a stagnation point is located on the discharge side rather than near the volute tongue, and the recirculation flow is very strong. This interferes with the outward flow from the impeller at the winding start of a volute and as a result the surrounding momentum decreases. Therefore, it is assumed that the momentum that flows out of areas other than the winding start of a volute is relatively large, and that the time-averaged value changes in direction at the winding start of a volute, as shown in Fig. 11(b). On the other hand, at large flow rate $\varphi = 0.047$, a stagnation point is located near the winding start of a volute, and it is flowing into the discharge side in large quantities, including the winding start of a volute. Therefore, it is thought that the time-averaged value changes in a counter direction to the discharge port.

Figure 11(c) shows that the fluctuating component ΔF_P of the pressure component is larger than the fluctuating component of the other components at all flow rates. The change in the time-averaged pressure component value obtained by the CFD analysis approximately agrees with the change in the time-averaged radial thrust values obtained by the CFD analysis (direct integration values) shown in Fig. 8(b). This shows that the pressure component is dominant in the time-averaged value of radial thrust.

Figures 13(a) to 13(d) show the results of the CFD analysis on the static pressure distributions at the cross section at the width center b/b_2 of the impeller outlet at different impeller phase angles θ_0 at a large flow rate $\varphi = 0.047$. Figures 13(a) to 13(d) show how the change in the impeller phase angle θ_0 causes the pressure coefficient C_P around the impeller to change significantly. C_P around the impeller is small at $\theta_0 = 180°$ but large at $\theta_0 = 0°$. In particular, a high-pressure domain exists at $30° < \theta < 180°$. This suggests that a large force acts toward the volute outlet region. This corresponds to the change in the pressure component F_P at the large flow rate $\varphi = 0.047$ shown in Fig. 11(c).

Summarizing the above results, the pressure component is the largest component in radial thrust, and it is dominant in affecting the change in the time-averaged value of the radial thrust and the magnitude and direction of the fluctuating component. The momentum component is considerably smaller than the other components, and decreases even further as the flow rate increases. The time-averaged values of the inertia component do not change significantly with the flow rate changes. The magnitude of the fluctuating component of the inertia component is comparable to that of the pressure component at a low flow rate and decreases slightly as the flow rate increases. Therefore, the reason for radial thrust cannot be estimated from the pressure distribution around the impeller in a single-blade pump is that the inertia component is large.

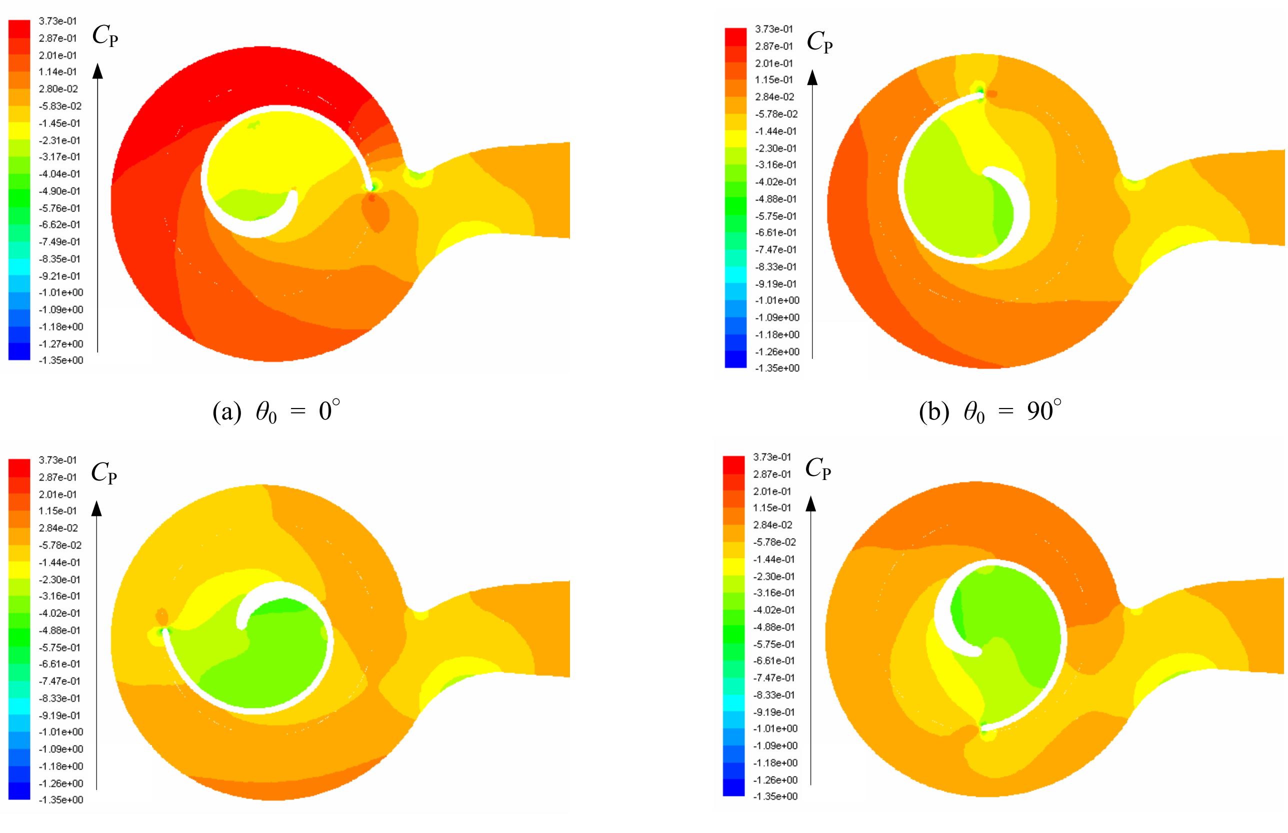

(a) $\theta_0 = 0^\circ$ (b) $\theta_0 = 90^\circ$ (c) $\theta_0 = 180^\circ$ (d) $\theta_0 = 270^\circ$

Fig. 13 Static pressure distributions ($\varphi = 0.047$)

5. Conclusion

A study on the radial thrust of a single-blade centrifugal pump yielded the following findings.

(1) The fluctuating components of radial thrust increase as the flow rate deviates from the design flow rate to a low or high value.

(2) The law of conservation of unsteady momentum was applied to the impeller used in this study to model radial thrust into inertia, momentum, and pressure components. The sum of these components agreed well with the radial thrust as calculated by integrating the pressure and the shearing stress on the impeller surface.

(3) The time-averaged values of the inertia component do not change significantly with the flow rate changes. Its fluctuating component has a magnitude nearly comparable with the pressure component at a low flow rate and decreases slightly as the flow rate increases. Because this inertia component is large, radial thrust cannot be estimated from the pressure distribution around the impeller in a single-blade pump.

(4) The change in the time-averaged value of the momentum component is different from that of the radial thrust. The magnitude of the fluctuating component of the momentum component is considerably smaller than the fluctuating components of other components, and decreases further with increase in the flow rate.

(5) The pressure component has the greatest effect on the time-averaged value and the fluctuating component of radial thrust. In the change in the time-averaged value of radial thrust with change in flow rate, the effect of the time-averaged value of the pressure component is dominant. The fluctuating components of the pressure component increase with the increase in flow rate.

Nomenclature

A	Area of the impeller [m^2]	Q	Flow rate [m^3/s]
b	Blade width [m]	r	Impeller radius [m]
C_P	Pressure coefficient ($=(P-P_s)/(\rho u_2^2/2)$)	u	Circumferential velocity [m/s]
D	Blade diameter [m]	v	Absolute velocity [m/s]
F	Radial thrust [N]	w	Relative velocity [m/s]
f	Radial thrust coefficient ($=F/(\rho u_2^2 b_2 r_2/2)$)	β_b	Blade angle [deg]
g	Gravitational acceleration [m/s^2]	η	Pump efficiency ($=\rho gQH/L$)
H	Total head [m]	λ	Shaft power coefficient ($=L/(\rho\pi D_2 b_2 u_2^3/2)$)
L	Shaft power [W]	ρ	Fluid density [kg/m^3]
n	Rotational speed [min^{-1}]	φ	Flow rate coefficient ($=Q/(\pi D_2 b_2 u_2)$)
P	Static pressure [Pa]	ψ	Head coefficient ($=H/(u_2^2/2g)$)
P_s	Static pressure at suction side reference position [Pa]		

Subscripts

0, 1, 2	Impeller suction inlet, Blade inlet, Blade outlet	*u*	Circumferential component
a	Axial component	*x*	x component
r	Radial component	*y*	y component

References

[1] Okamura, T., 1979. “Radial Thrust in Centrifugal Pumps with Single Vane Impeller,” Transactions of the Japan Society of Mechanical Engineers, Series B, Vol. 45, No. 398, p. 1458. (in Japanese)

[2] Aoki, M., 1984. “Instantaneous Inter-Blade Pressure Distributions and Fluctuating Radial Thrust in a Single-Blade Centrifugal Pump,” Transactions of the Japan Society of Mechanical Engineers, Series B, Vol. 50, No. 451, p. 661. (in Japanese)

[3] Stepanoff, A. J., 1967. “Centrifugal and Axial Flow Pumps,” p. 116, John Wiley & Sons.

[4] Agostinelli, A., Nobles, D. and Mockridge, C. R., 1960. “An Experimental Investigation of Radial Thrust in Centrifugal Pumps,” Transactions of the American Society of Mechanical Engineers, Vol. 82, No. 2, p. 120.

[5] Biheller, H. J., 1965. “Radial Force on the Impeller of Centrifugal Pumps with Volute, Semivolute, and Fully Concentric Casings,” Transactions of the American Society of Mechanical Engineers, Series A, Vol. 87, No. 3, p. 319.

[6] Imaichi, K., Uchida, N. and Shirai, T., 1971. “An Experimental Investigation on the Radial Thrust in a Centrifugal Pump,” Transactions of the Japan Society of Mechanical Engineers, Vol. 37, No. 294, p. 322. (in Japanese)

[7] Yoshida, Y., Sakatani, T., Kawakami, T. and Tsujimoto, Y., 1995. “Study of Hydraulic Unbalance Caused by Geometrical Manufacturing Errors of Centrifugal Impeller (1st Report: Experimental Results),” Turbomachinery, Vol. 23, No. 2, p. 72. (in Japanese)

[8] Benra, F.-K., Dohmen H.J. and Schneider O., 2003. “Calculation of Hydrodynamic Forces and Flow Induced Vibrations of Centrifugal Sewage Water Pumps,” 4th ASME/JSME Joint Fluids Engineering Conference, Paper FEDSM2003-45102, Honolulu, Hawaii, USA.

[9] Benra, F.-K., Dohmen H.J. and Sommer M., 2006. “Experimental Investigation of Hydrodynamic Forces for Different Configurations of Single-Blade Centrifugal Pumps,” The 11th International Symposium on Transport Phenomena and Dynamics of Rotating Machinery (ISROMAC-11), Honolulu, Hawaii, USA.

[10] Nishi, Y., Fujiwara, R. and Fukutomi, J., 2009. “Design Method for Single-Blade Centrifugal Pump Impeller,” Transactions of the Japan Society of Mechanical Engineers, Series B, Vol. 75, No. 754, p. 106. (in Japanese)

[11] Tanaka, K., Arai, M., Ikeo, S. and Matsumoto, Y., 1989. “Radial Thrust in Screw Centrifugal Pump Impeller,” Turbomachinery, Vol. 17, No. 4, p. 215. (in Japanese)

[12] Ishida, I., 2002. “The Consideration in the Radial Thrust Decrease of Centrifugal Pump,” Turbomachinery, Vol. 30, No. 12, p. 741. (in Japanese)

[13] Nishi, Y., Matsuo, N. and Fukutomi, J., 2008. “A Study on Internal Flow in a New Type of Sewage Pump (1st Report, Comparison between Experiment and CFD Calculation),” Transactions of the Japan Society of Mechanical Engineers, Series B, Vol. 74, No. 742, p. 1386. (in Japanese)

[14] Fluent User’s Manual, 2006. pp. 9-30. (in Japanese)

[15] Worster, R. C., 1963. “The Flow in Volutes and its Effect on Centrifugal Pump Performance,” Proc. Instn. Mech. Engrs., Vol. 177, No. 31, p. 843.

[16] Nishi, Y., Makita, K. and Fukutomi, J., 2006. “A Study on a New Type of Sewage Pump,” Transactions of the Japan Society of Mechanical Engineers, Series B, Vol. 72, No. 720, p. 1984. (in Japanese)